Featured in Physics

Forward and Inverse Energy Cascade in Fluid Turbulence Adhere to Kolmogorov's Refined Similarity Hypothesis

H. Yao
Department of Mechanical Engineering & Institute for Data Intensive Engineering & Science, Johns Hopkins University, 3400 N. Charles Street, Baltimore, Maryland 21218, USA

P. K. Yeung
Department of Aerospace Engineering and Mechanical Engineering, Georgia Institute of Technology, North Avenue, Atlanta, Georgia 30332, USA

T. A. Zaki and C. Meneveau*
Mechanical Engineering & IDIES, Johns Hopkins University, 3400 N. Charles Street, Baltimore, Maryland 21218, USA

(Received 25 September 2023; accepted 28 February 2024; published 17 April 2024)

We study fluctuations of the local energy cascade rate Φ_ℓ in turbulent flows at scales (ℓ) in the inertial range. According to the Kolmogorov refined similarity hypothesis (KRSH), relevant statistical properties of Φ_ℓ should depend on ϵ_ℓ, the viscous dissipation rate locally averaged over a sphere of size ℓ, rather than on the global average dissipation. However, the validity of KRSH applied to Φ_ℓ has not yet been tested from data. Conditional averages such as $\langle \Phi_\ell | \epsilon_\ell \rangle$ as well as of higher-order moments are measured from direct numerical simulations data, and results clearly adhere to the predictions from KRSH. Remarkably, the same is true when considering forward ($\Phi_\ell > 0$) and inverse ($\Phi_\ell < 0$) cascade events separately. Measured ratios of forward and inverse cascade probability densities conditioned on ϵ_ℓ also confirm the applicability of the KRSH to analysis of the fluctuation relation from nonequilibrium thermodynamics.

DOI: 10.1103/PhysRevLett.132.164001

The classic description of the energy cascade in turbulent flows states that the turbulent kinetic energy is extracted from large-scale eddies, transferred to smaller scale eddies, and finally dissipated into heat due to viscous friction [1]. What is known from the Navier-Stokes equations is the celebrated $-4/5$ law [2,3], $\langle \delta u_{\rm ll}^3(r) \rangle \equiv \langle ([\mathbf{u}(\mathbf{x}+\mathbf{r}) - \mathbf{u}(\mathbf{x})] \cdot \mathbf{r}/r)^3 \rangle = -(4/5) r \langle \epsilon \rangle$. Here, $\langle .. \rangle$ denotes statistical averaging, $\delta u_{\rm ll}(r)$ is the longitudinal velocity increment over distance r, ϵ is the viscous dissipation rate, and $r = |\mathbf{r}|$ is assumed to be inside the inertial range. The $4/5$ law means that in the inertial range, $-(5/4)\langle \delta u_{\rm ll}^3 \rangle / r$ can be interpreted as the energy cascade rate and that the average direction of the cascade is from large to small scales. However, it is well known that $\delta u_{\rm ll}$ and ϵ display strong intermittency [3–5]. To describe intermittency and anomalous scaling, Kolmogorov's second refined similarity hypothesis (KRSH) [4] connects the statistics of $\delta u_{\rm ll}(r)$ to the local dissipation ϵ_r, defined as the pointwise dissipation averaged in a ball of diameter r. KRSH has received strong support from early experimental measurements in which the dissipation ϵ_r had to be approximated by lower-dimensional data (e.g., [6,7]) and also from later analyses based on 3D data, in which ϵ_r could be evaluated fully, from simulations [8–10] or recent 3D experimental data [11].

Most prior studies have started out with the KRSH formulated as a hypothesis inspired by dimensional analysis, but direct connections between KRSH and first principles Navier-Stokes equations have often been lacking. In this Letter, we revisit the equation of Hill [12], from which a quantitative definition of the local cascade rate is possible. In this context we test the validity of the KRSH using conditional averaging based on local dissipation. We extend the analysis and show new results concerning the probabilities of forward and inverse cascade rates.

The equation derived by Hill [12], for scales at which forcing can be neglected, and before averaging, is of the form $\partial_t |\delta \mathbf{u}|^2 = -\boldsymbol{\nabla}_{\mathbf{r}} \cdot (\delta \mathbf{u} |\delta \mathbf{u}|^2) - 4\epsilon^* + \cdots$, where $\delta \mathbf{u}(\mathbf{x};\mathbf{r})$ is the velocity increment vector $\delta u_i(\mathbf{x};\mathbf{r}) = u_i^+ - u_i^-$ and the superscripts $+$ and $-$ represent two points $\mathbf{x} + \mathbf{r}/2$ and $\mathbf{x} - \mathbf{r}/2$ in the physical domain that have a separation vector $r_i = x_i^+ - x_i^-$ and middle point $x_i = (x_i^+ + x_i^-)/2$. $\epsilon^* = (\epsilon^+ + \epsilon^-)/2$ is the average dissipation, where ϵ denotes the "pseudo-dissipation," defined as $\epsilon = \nu(\partial u_i / \partial x_j)^2$. Many variants of this equation (also called Karman-Howarth-Monin-Hill (KHMH) equation in [13]) have been studied [14,15]. To make connection to the RKSH and ϵ_ℓ at some scale $r = \ell$, the Hill equation at any point $\mathbf{x}$ can be integrated over a sphere in scale $\mathbf{r}$ space up to a diameter $r = \ell$. The resulting equation

describes the evolution of local kinetic energy up to scale ℓ defined as $k_\ell = (1/2\Omega_\ell)\int_{\Omega_\ell}\frac{1}{2}\delta u_i^2 d^3\mathbf{r}_s$ with the radius vector $\mathbf{r}_s = \mathbf{r}/2$ integrated up to $\ell/2$. When divided by the volume of the sphere $[\Omega_\ell = \frac{4}{3}\pi(\ell/2)^3]$ and a factor of 4, the locally integrated form of the Hill equation becomes

$$\frac{\tilde{d}k_\ell}{dt} = \Phi_\ell + P_\ell + D_\ell - \epsilon_\ell, \tag{1}$$

where $\epsilon_\ell(\mathbf{x}) \equiv (1/\Omega_\ell)\int_{\Omega_\ell}\epsilon^*(\mathbf{x},\mathbf{r})d^3\mathbf{r}_s$ is the ℓ-averaged dissipation envisioned in the RKSH, and

$$\Phi_\ell(\mathbf{x}) \equiv -\frac{3}{4\ell}\frac{1}{S_\ell}\oint_{S_\ell}\delta u_i^2\delta u_j\hat{n}_j dS \tag{2}$$

is interpreted as the local energy cascade rate where $\hat{\mathbf{n}} = \mathbf{r}/|\mathbf{r}|$ and $S_\ell = 4\pi(\ell/2)^2$. Equation (1) also includes $\tilde{d}k_\ell/dt$, the advective rate of change of kinetic energy k_ℓ, a surface averaged pressure work term P_ℓ at scale ℓ, as well as a scale and spatial viscous diffusion term D_ℓ (definitions are provided in Supplemental Material [16]). We consider ℓ to be in the inertial range, therefore D_ℓ is negligible. Equation (1), the "scale-integrated local KH" (Kolmogorov-Hill) equation is local, valid at any $(\mathbf{x}, t)$ (see also [17–19]).

A reformulation of the KRSH is that the statistics of Φ_ℓ only depend on the statistics of ϵ_ℓ (i.e., that $\Phi_\ell = V_\Phi\epsilon_\ell$ with random variable V_Φ independent of ℓ and ϵ_ℓ) in the inertial range. In particular, the conditional average of the cascade rate should obey $\langle\Phi_\ell|\epsilon_\ell\rangle = \epsilon_\ell$ and $\langle V_\Phi\rangle = 1$. In fact, referring back to Eq. (1), we may take its conditional average and write (neglecting D_ℓ, and using $\langle\epsilon_\ell|\epsilon_\ell\rangle = \epsilon_\ell$)

$$\langle\tilde{d}k_\ell/dt|\epsilon_\ell\rangle = \langle\Phi_\ell|\epsilon_\ell\rangle + \langle P_\ell|\epsilon_\ell\rangle - \epsilon_\ell. \tag{3}$$

Hence, a consequence of the KRSH with Eq. (1) is that the conditional average of $W_\ell \equiv \tilde{d}k_\ell/dt - P_\ell$ must vanish, i.e., $\langle W_\ell|\epsilon_r\rangle = 0$ (or both $\langle\tilde{d}k_\ell/dt|\epsilon_\ell\rangle = 0$ and $\langle P_\ell|\epsilon_\ell\rangle = 0$).

Prior measurements of Φ_ℓ [20,21] show that it can be both positive and negative locally, and moreover [21] suggests that the ratio $\Psi_\ell = \Phi_\ell/k_\ell$ can be understood as an entropy generation (or phase-space contraction) rate where, drawing an analogy between turbulent eddies and particle systems, k_ℓ is interpreted as the temperature of turbulence. The definition of Ψ_ℓ was inspired by the Gibbs equation in which the net entropy generation rate is related to the ratio of energy transfer rate divided by temperature (see [21] for more details). There is growing interest in connecting turbulence with thermodynamics concepts, e.g., focusing on model systems [22,23], and on possible definitions of entropy [24] and temperature [25]. A prediction about entropy generation rates in nonequilibrium thermodynamics is the "fluctuation relation" (FR) [26,27]. Prior authors have examined the FR, most often focusing on stochastic models [28] but also on fluctuations in global power input [29] and spectral energy transfer [30]. When written for the turbulence entropy generation rate as defined in [21] the FR states that the ratio of probability densities of positive and negative Ψ_ℓ follows the exponential behavior $P(\Psi_\ell)/P(-\Psi_\ell) = \exp(\Psi_\ell\tau_\ell)$, where τ_ℓ is a characteristic timescale. The recent results of [21] provide direct empirical evidence for the applicability of the FR relationship for isotropic turbulence, i.e., they observed that $\ln[P(\Psi_\ell)/P(-\Psi_\ell)]$ followed a mostly linear behavior with Ψ_ℓ. Interestingly, they found that division by "temperature" k_ℓ was necessary to observe behavior consistent with the FR. Without such division, the ratio of probabilities deviated far more significantly from linear behavior. However, in the prior analysis [21], the timescale used to normalize Ψ_ℓ was defined using the average dissipation rate, i.e., $\bar{\tau}_\ell = \langle\epsilon\rangle^{-1/3}\ell^{2/3}$. In other words, it did not take into account effects of intermittency in which different regions of the flow with different ϵ_ℓ values could (according to KRSH) behave differently.

The specific aims in this Letter are to investigate whether data support the KRSH in the context of the dynamics of turbulent kinetic energy at scale ℓ as described by Eq. (1), i.e., whether predictions from KRSH hold for (i) conditional moments of Φ_ℓ, (ii) for the combined unsteady and pressure terms W_ℓ, (iii) for positive and negative cascade rates, and (iv) for cascade rate probability ratios motivated by the fluctuation relation from nonequilibrium thermodynamics.

We evaluate terms in Eq. (1) using data from direct numerical simulation of isotropic turbulence at $R_\lambda \approx 1,250$ (data obtained from the Johns Hopkins Turbulence Database (JHTDB) [31,32]). Surface averages of Φ_ℓ are measured by discretizing the outer surface of diameter ℓ into 500 point pairs (+ and − points) that are approximately uniformly distributed on the sphere. Velocities for δu_i are downloaded from JHTDB. Volume integrals ϵ_ℓ and k_ℓ are evaluated similarly by integrating over five concentric spheres. The accuracy of this method of integration has been tested by increasing the number of points used in the discretization and confirming indistinguishable results are obtained. For ϵ we use JHTDB's GetVelocityGradient method with 4th-order centered finite differencing. Taking dissipation as an example, panel (a) in Fig. 1 shows pointwise normalized dissipation $\epsilon(\mathbf{x})/\langle\epsilon\rangle$ computed on a planar cut across the data (the plane shown corresponds to 500×500 grid points). Panel (b) of Fig. 1 shows a sphere with diameter ℓ.

Figure 2 shows the conditional average $\langle\Phi_\ell|\epsilon_\ell\rangle$ as function of ϵ_ℓ. Statistics are computed using 2 000 000 randomly distributed spheres across the entire 8192^3 isotropic turbulence dataset (isotropic8192) [32]. The analysis considers two length scales in the inertial range and one approaching the viscous range, namely $\ell = 0.024L = 60\eta$, $\ell = 0.018L = 45\eta$, and $\ell = 0.012L = 30\eta$,

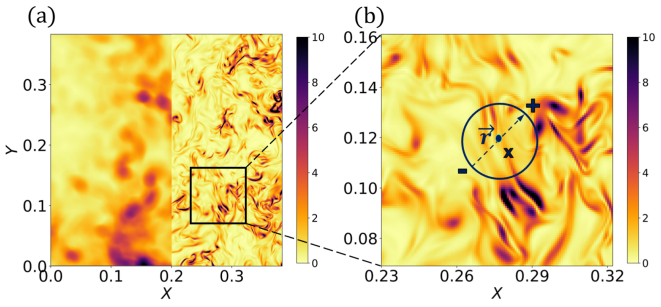

FIG. 1. (a) Spatial distribution of local dissipation rate normalized by $\langle\epsilon\rangle$ on a plane in a small subset of isotropic turbulence at $R_\lambda = 1250$. The left portion shows ϵ_ℓ distribution obtained from spherical filtering. (b) Close-up portion of panel (a) also showing a sphere with a diameter $\ell = 45\eta$ marked as the black circle. The black dash arrow represents $\mathbf{r}$ separating the two points $+$ and $-$.

respectively, where $L = 1.24$ is the integral scale and the Kolmogorov scale is $\eta = (\nu^3/\langle\epsilon\rangle)^{1/4} = 4.98 \times 10^{-4}$. It is apparent that the dominant terms are $\langle\Phi_\ell|\epsilon_\ell\rangle$ (black symbols and lines) and ϵ_ℓ itself (red dash line with unit slope). These are equal for most of the range of ϵ_ℓ for which reliable statistics can be collected. The good collapse $\langle\Phi_\ell|\epsilon_\ell\rangle \approx \epsilon_\ell$ provides clear support for the KRSH in the context of terms appearing in Eq. (1). Also plotted in Fig. 2 are the conditional averages of the pressure term $\langle P_\ell|\epsilon_\ell\rangle$ and the viscous term $\langle D_\ell|\epsilon_\ell\rangle$. We can see that the contribution of the pressure term (yellow symbols and lines) is negligible at all three length scales over most of the range. The viscous term (blue symbols and lines) is also negligibly small as expected. Approaching the largest values of $\epsilon_\ell/\langle\epsilon\rangle$ we observe saturation of Φ_ℓ that is compensated by a small rise of the pressure term [same

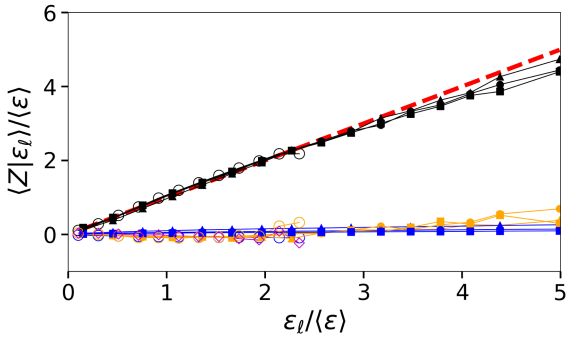

FIG. 2. Conditional averages of terms in the scale-integrated local KH equation based on ϵ_ℓ, i.e., $Z = \Phi_\ell$ (black symbols and lines), $Z = P_\ell$ (yellow symbols and lines), $Z = D_\ell$ (blue symbols and lines). The red dashed line indicates ϵ_ℓ. Different symbols denote different scales $\ell/L = 0.012$ [triangles, (30η)], 0.018 [circles, (45η)], and 0.024 [squares, (60η)]. Data is from DNS at $R_\lambda = 1,250$ (solid symbols) and $R_\lambda = 430$ at $\ell/L = 0.092(45\eta)$ (open circles), for which $Z = \tilde{d}k_\ell/dt$ (purple diamonds) is included.

results are obtained when using the full viscous dissipation $\nu\partial u_i/\partial x_j(\partial u_i/\partial x_j + \partial u_j/\partial x_i)$ instead of the pseudo-dissipation $\nu(\partial u_i/\partial x_j)^2$].

Moreover, based on Eq. (3), we can conclude that $\langle\tilde{d}k_\ell/dt|\epsilon_\ell\rangle \approx 0$, given that $\langle P_\ell|\epsilon_\ell\rangle \approx 0$, $\langle D_\ell|\epsilon_\ell\rangle \approx 0$, and $\langle\Phi_\ell|\epsilon_\ell\rangle \approx \epsilon_\ell$. To verify this result via explicit measurement, we computed the terms in Eq. (3) using the isotropic1024 [31] dataset. It has a smaller size of 1024^3 grid points and a lower Reynolds number $R_\lambda = 430$, but includes temporally consecutive snapshots allowing us to calculate time derivatives. Figure 2 (open symbols) shows that $\langle\Phi_\ell|\epsilon_\ell\rangle \approx \epsilon_\ell$ still holds very well at this lower Reynolds number, that the pressure and viscous terms are again close to zero, and that $\langle\tilde{d}k_\ell/dt|\epsilon_\ell\rangle \approx 0$. We conclude that the data provide strong direct support to the KRSH relating Φ_ℓ and ϵ_ℓ and that the pressure and unsteadiness terms vanish in the inertial range.

A further implication of KRSH relates to higher order moments. It implies that $\langle\Phi_\ell^q|\epsilon_\ell\rangle = \langle V_\Phi^q\rangle\epsilon_\ell^q$. In the inertial range, since $\Phi_\ell = \epsilon_\ell + W_\ell$ locally and instantaneously, raising to the q power, expanding, and taking the conditional average yields $\langle\Phi_\ell^q|\epsilon_\ell\rangle = \sum_{n=0}^{q}\binom{q}{n}\epsilon_\ell^{q-n}\langle W_\ell^n|\epsilon_\ell\rangle$. Thus, for KRSH to hold (i.e., for $\langle\Phi_\ell^q|\epsilon_\ell\rangle \propto \epsilon_\ell^q$) the conditional moments of W_ℓ must follow the same behavior, i.e., $\langle W_\ell^n|\epsilon_\ell\rangle \propto \epsilon_\ell^n$. Both the KRSH prediction for $\langle\Phi_\ell^q|\epsilon_\ell\rangle$ and $\langle W_\ell^n|\epsilon_\ell\rangle$ can be tested by measuring and plotting $\langle\Phi_\ell^q|\epsilon_\ell\rangle^{1/q}$ and $\langle W_\ell^n|\epsilon_\ell\rangle^{1/n}$ as function of ϵ_ℓ and testing for linear behavior. Results are shown in Fig. 3 for $q = 2, 3$ and $n = 2, 3$. Clearly, the proportionality holds, with linear trends visible for these moment orders over the range of dissipation values.

We now turn to further consequences of the KRSH that are directly related to the direction of the energy cascade, i.e., we examine if KRSH may be applicable even to those regions of the flow where $\Phi_\ell < 0$, i.e., those displaying only inverse cascading, or $\Phi_\ell > 0$, i.e., those displaying only forward cascading. An implication of KRSH is that the conditional average of only positive and only negative values of Φ_ℓ should also be proportional to ϵ_ℓ. To investigate this prediction, we split the samples of Φ_ℓ by

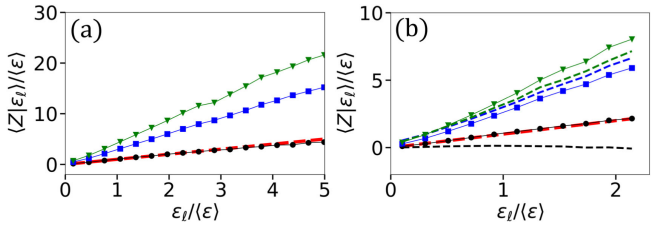

FIG. 3. Conditional averaged $Z = \Phi_\ell^q$ (symbols) for the isotropic8192 (a) and isotropic1024 (b) datasets, and $Z = W_\ell^n$ (dashed lines for the isotropic1024 dataset), for $\ell = 45\eta$, plotted as function of ϵ_ℓ. Results for q, $n = 1, 2, 3$ are shown in black, blue, and green, respectively. All terms display linear trends with ϵ_ℓ, consistent with the KRSH.

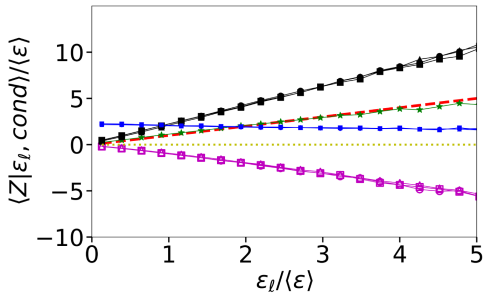

FIG. 4. Conditionally averaged positive (forward cascade, full symbols, $Z = \Phi_\ell$, cond: $\Phi_\ell > 0$) and negative (inverse cascade, empty symbols, $Z = \Phi_\ell$, cond: $\Phi_\ell < 0$) for the isotropic8192 dataset, and for three scales ℓ (symbols are the same as in Fig. 2). The green stars show the standard 4/5-law quantity based on longitudinal structure function, i.e., for $Z = (-5/4\ell)(\delta u_j \hat{n}_j)^3$, and no additional condition beyond ϵ_ℓ. Blue symbols is $\Pr(\Phi_\ell > 0|\epsilon_\ell)/\Pr(\Phi_\ell < 0|\epsilon_\ell)$ (≈2.0).

its sign and perform conditional averaging based on ϵ_ℓ. We first observe that there are about twice as many samples with $\Phi_\ell > 0$ than with $\Phi_\ell < 0$, specifically, if $\Pr(\Phi_\ell > 0|\epsilon_\ell)$ and $\Pr(\Phi_\ell < 0|\epsilon_\ell)$ are the conditional total probabilities associated with signs of Φ_ℓ in any ϵ_ℓ bin, we measure $\Pr(\Phi_\ell > 0|\epsilon_\ell)/\Pr(\Phi_\ell < 0|\epsilon_\ell) \approx 2.0$ (see blue line in Fig. 4). In the inertial range, the ratio is approximately 2.0 (consistent with results from Ref. [33], who defined the energy cascade rate by detailed evaluations of the intersection of eddies and lifetimes). From normalization we conclude that $\Pr(\Phi_\ell > 0|\epsilon_\ell) \approx 2/3$ and $\Pr(\Phi_\ell < 0|\epsilon_\ell) \approx 1/3$. And since $\langle\Phi_\ell|\epsilon_\ell\rangle = \langle\Phi_\ell|\epsilon_\ell, \Phi_\ell > 0\rangle \Pr(\Phi_\ell > 0|\epsilon_\ell) + \langle\Phi_\ell|\epsilon_\ell, \Phi_\ell < 0\rangle \Pr(\Phi_\ell < 0|\epsilon_\ell)$ and the data already showed $\langle\Phi_\ell|\epsilon_\ell\rangle \approx \epsilon_\ell$, the KRSH further implies that $\langle\Phi_\ell|\epsilon_\ell, \Phi_\ell < 0\rangle \approx 3\epsilon_\ell - 2\langle\Phi_\ell|\epsilon_\ell, \Phi_\ell > 0\rangle$. These predictions from RKSH are tested in Fig. 4, showing that $\langle\Phi_\ell|\epsilon_\ell, \Phi_\ell > 0\rangle \approx 2\epsilon_\ell$ and $\langle\Phi_\ell|\epsilon_\ell, \Phi_\ell < 0\rangle \approx -1\epsilon_\ell$. Clearly, KRSH holds even for the positive and negative regions separately. For completeness, we also show the conditional average of the traditional third-order longitudinal structure function, which under the assumption of isotropy and KRSH follows $-(5/4\ell)\langle(\delta u_j \hat{n}_j)^3|\epsilon_\ell\rangle = \epsilon_\ell$.

Next, following Ref. [21] we examine the fluctuation relation from nonequilibrium thermodynamics for the normalized entropy generation rate $\Psi_\ell \tau_\ell$, but instead of using the overall dissipation rate to define the characteristic eddy turnover timescale, we here use conditioning on various values of local dissipation ϵ_ℓ. Figure 5(a) shows the conditional probability density function (PDF) $P(\Psi_\ell|\epsilon_\ell)$ of the entropy generation rate $\Psi_\ell = \Phi_\ell/k_\ell$ for $\ell/\eta = 45$, conditioned for various values of ϵ_ℓ ranging from $\epsilon_\ell/\langle\epsilon\rangle = 0.15$ to 4.2. As in [21], exponential tails are found, with steeper slopes on the negative side than on the positive one, and approximately twice as steep. Remarkably, when multiplying Ψ_ℓ by the corresponding local turnover timescale $\tau_\ell = \epsilon_\ell^{-1/3}\ell^{2/3}$ where ϵ_ℓ is the value used to bin the data, excellent collapse is observed, see Fig. 5(b). If the PDFs are approximated as pure exponentials, with slope magnitudes α_- for $\Psi_\ell < 0$ and α_+ for $\Psi_\ell > 0$, it is evident from Fig. 5(b) that $\alpha_+ \approx 1$ and $\alpha_- \approx 2$. For such two-sided exponential PDFs, it is easy to show that $\Pr(\Psi_\ell < 0)/\Pr(\Psi_\ell > 0) = \alpha_+/\alpha_-$, consistent with the 1:2 ratio discussed above, independent of ϵ_ℓ. Finally, the FR can be tested by plotting $\log[P(\Psi_\ell|\epsilon_\ell)/P(-\Psi_\ell|\epsilon_\ell)]$ versus $\Psi_\ell\tau_\ell$ (see Fig. 6). The result shows good collapse and an approximately linear trend (especially at $\Psi_\ell\tau_\ell > 1$), thus providing empirical and approximate support for the fluctuation relation for turbulence even when conditioning on different values of ϵ_ℓ, and using ϵ_ℓ to establish the relevant turnover timescale. For the exponential approximation of the conditional PDFs, the slope in the FR plot is simply $\alpha_- - \alpha_+$, which is nearly unity (as observed originally in [21]), and quite consistent with $\alpha_- \approx 2$ while $\alpha_+ \approx 1$.

In summary, we examined the KRSH involving the local dissipation ϵ_ℓ in the context of an equation [Eq. (1)] derived exactly from the Navier-Stokes equations. Results from two DNS of forced isotropic turbulence provided strong support for the validity of KRSH for the cascade rate Φ_ℓ, its moments, and also for moments of other terms appearing in the dynamical equation. Furthermore the data support a strong version of the KRSH when positive and negative cascade rates are considered separately, each of which scale proportional to ϵ_ℓ. Finally, ratios of probabilities of forward and inverse cascade rates are shown to collapse well when invoking the KRSH [Fig. 5(b)]. The so collapsed PDFs

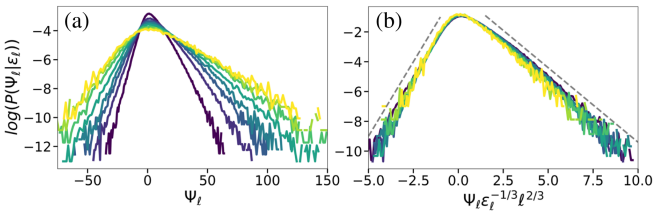

FIG. 5. Conditional PDFs of Ψ_ℓ, for $\ell = 45\eta$ conditioned on ranges in bins centered at $\epsilon_\ell/\langle\epsilon\rangle = 0.15$ (black), 0.45, 0.75, 1.05, 1.8, 3.0, 4.2, and 5.4 (yellow). The gray dashed lines have slopes = 2 (left) and −1 (right). A natural logarithm is used.

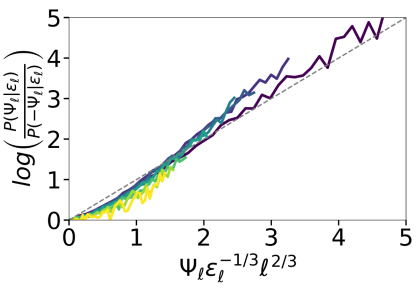

FIG. 6. Test of conditional FR for different values of $\epsilon_\ell/\langle\epsilon\rangle$ (same line colors as in Fig. 5). The gray line has slope = 1.

display exponential tails that yield results consistent with the FR from nonequilibrium thermodynamics. Present findings connecting KRSH directly to a dynamical equation derived from the Navier-Stokes equations could help in developing improved theories and models of the turbulence cascade process and establish new links between turbulence and nonequilibrium thermodynamics.

Additional questions arise, such as what occurs when ℓ approaches limits of the inertial range, what are possible effects of Reynolds number (recall that present results in Figs. 2 and 3 are for two Reynolds numbers only), and, do the results hold for flows with mean shear and walls? Regarding the analysis of entropy generation rate, we have tested the FR only as far as the fluctuations in Ψ_ℓ are concerned, setting $t = \tau_\ell$, which raises the question of what are the effects of time averaging? It also bears recalling that while the FR was originally derived for the entropy generation rate in systems in which the microscopic dynamics are time reversible [26,27], more general versions have been developed since [34,35]. Nonetheless, as in [21] we here regard the microscopic degrees of freedom to be the inertial-range eddies smaller than ℓ whose evolution is governed by nearly inviscid, thus time-reversible, dynamics at least for some small finite time. While the actual turbulent state we are analyzing is already far from equilibrium so that the overall statistics of velocity increments (and Φ_ℓ, Ψ_ℓ) display the established asymmetry, the actual dynamics in the inertial range can be time reversed for some time [24]. Still, significant questions remain about connections between nonequilibrium thermodynamics and 3D turbulence in the inertial range.

We thank Reginald J. Hill for comments on an early draft of this work. The work is supported by National Science Foundation (CSSI-2103874) and the contributions from the JHTDB team are gratefully acknowledged.

*meneveau@jhu.edu

[1] L. F. Richardson, *Weather Prediction by Numerical Process* (Cambridge University Press, Cambridge, England, 1922), 10.1017/CBO9780511618291.
[2] A. N. Kolmogorov, C.R. Acad. Sci. URSS **30**, 301 (1941).
[3] U. Frisch, *Turbulence: The Legacy of AN Kolmogorov* (Cambridge University Press, Cambridge, England, 1995).
[4] A. N. Kolmogorov, J. Fluid Mech. **13**, 82 (1962).
[5] C. Meneveau and K. R. Sreenivasan, J. Fluid Mech. **224**, 429 (1991).
[6] G. Stolovitzky, P. Kailasnath, and K. R. Sreenivasan, Phys. Rev. Lett. **69**, 1178 (1992).
[7] A. A. Praskovsky, Phys. Fluids A **4**, 2589 (1992).
[8] L.-P. Wang, S. Chen, J. G. Brasseur, and J. C. Wyngaard, J. Fluid Mech. **309**, 113 (1996).
[9] K. P. Iyer, K. R. Sreenivasan, and P. K. Yeung, Phys. Rev. E **92**, 063024 (2015).
[10] P. K. Yeung and K. Ravikumar, Phys. Rev. Fluids **5**, 110517 (2020).
[11] J. M. Lawson, E. Bodenschatz, A. N. Knutsen, J. R. Dawson, and N. A. Worth, Phys. Rev. Fluids **4**, 022601 (R) (2019).
[12] R. J. Hill, J. Fluid Mech. **468**, 317 (2002).
[13] T. Yasuda and J. C. Vassilicos, J. Fluid Mech. **853**, 235 (2018).
[14] A. S. Monin and A. M. Yaglom, *Statistical Fluid Mechanics: Mechanics of Turbulence* (MIT Press, Cambridge, MA, 1975).
[15] L. Danaila, F. Anselmet, T. Zhou, and R. A. Antonia, J. Fluid Mech. **430**, 87 (2001).
[16] See Supplemental Material at http://link.aps.org/supplemental/10.1103/PhysRevLett.132.164001 for definitions of the various terms in the original Hill equation and the terms in Eq. (1), as well as details about how Eq. (1) is derived.
[17] J. Duchon and R. Robert, Nonlinearity **13**, 249 (2000).
[18] G. L. Eyink, Nonlinearity **16**, 137 (2002).
[19] B. Dubrulle, J. Fluid Mech. **867**, P1 (2019).
[20] H. Yao, M. Schnaubelt, A. S. Szalay, T. A. Zaki, and C. Meneveau, J. Fluid Mech. **980**, A42 (2024).
[21] H. Yao, T. A. Zaki, and C. Meneveau, J. Fluid Mech. **973**, R6 (2023).
[22] A. J. Chorin, Commun. Math. Phys. **141**, 619 (1991).
[23] G. Paladin and A. Vulpiani, Phys. Rep. **156**, 147 (1987).
[24] A. Vela-Martín and J. Jiménez, J. Fluid Mech. **915**, A36 (2021).
[25] B. Castaing, J. Phys. II (France) **6**, 105 (1996).
[26] D. J. Evans, E. G. D. Cohen, and G. P. Morriss, Phys. Rev. Lett. **71**, 2401 (1993).
[27] G. Gallavotti and E. G. D. Cohen, Phys. Rev. Lett. **74**, 2694 (1995).
[28] A. Fuchs, S. M. D. Queirós, P. G. Lind, A. Girard, F. Bouchet, M. Wächter, and J. Peinke, Phys. Rev. Fluids **5**, 034602 (2020).
[29] F. Zonta and S. Chibbaro, Europhys. Lett. **114**, 50011 (2016).
[30] A. Porporato, M. Hooshyar, A. D. Bragg, and G. Katul, Proc. R. Soc. A **476**, 20200468 (2020).
[31] Y. Li, E. Perlman, M. Wan, Y. Yang, C. Meneveau, R. Burns, S. Chen, A. Szalay, and G. Eyink, J. Turbul. **9**, N31 (2008).
[32] P. K. Yeung, X. M. Zhai, and K. R. Sreenivasan, Proc. Natl. Acad. Sci. U.S.A. **112**, 12633 (2015).
[33] J. I. Cardesa, A. Vela-Martín, and J. Jiménez, Science **357**, 782 (2017).
[34] V. Y. Chernyak, M. Chertkov, and C. Jarzynski, J. Stat. Mech. (2006) P08001.
[35] G. Gallavotti, Eur. Phys. J. E **43**, 37 (2020).